Journal of Power Sources 644 (2025) 236925

Contents lists available at ScienceDirect

Journal of Power Sources

journal homepage: www.elsevier.com/locate/jpowsour

Expanding the electrochemical stable window of aqueous-based electrolytes via competitive solvation induced by aprotic solvents

Yibing Yang [a,1], Jiapei Li [b,1], Junlin Shi [a], Fei Pan [c], Shuilin Wu [a,*], Daohong Zhang [a], Yanwu Zhu [c], Wenjun Zhang [b,**]

[a] Key Laboratory of Catalysis and Energy Materials Chemistry of Ministry of Education & Hubei Key Laboratory of Catalysis and Materials Science, South-Central Minzu University, Wuhan, 430074, China
[b] Department of Materials Science and Engineering, and Center of Super-Diamond and Advanced Films, City University of Hong Kong, 83 Tat Chee Avenue, Hong Kong, China
[c] School of Chemistry and Materials Science, University of Science and Technology of China, Hefei, 230026, China

HIGHLIGHTS

- Competitive solvation was used to expand electrochemical window of water.
- Aprotic solvents' capabilities in expanding electrochemical window are varied.
- A 2.6V aqueous-based supercapacitor was developed.

GRAPHICAL ABSTRACT

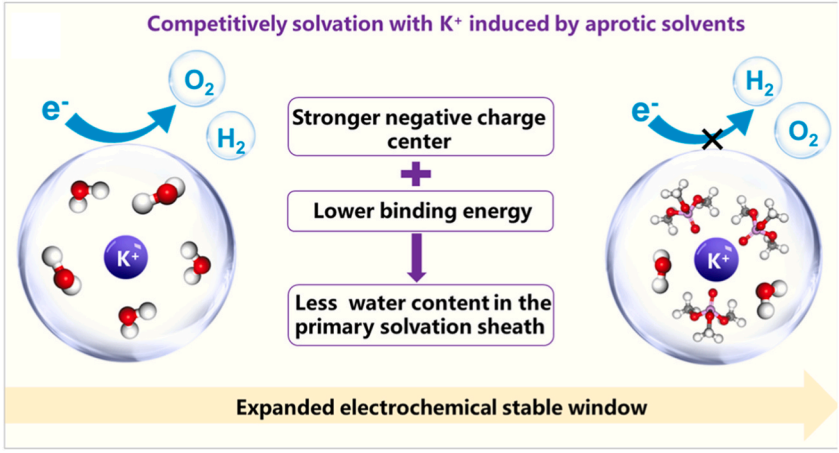

ARTICLE INFO

Keywords:
Electrolyte engineering
Competitive solvation
Aqueous supercapacitors

ABSTRACT

Aqueous electrolytes offer a promising alternative for safe, cost-effective, and scalable energy storage. However, the narrow electrochemical window of water limits their widespread application. Using super-concentrated electrolytes can effectively expand the aqueous electrolytes' electrochemical window, but the use of excessive salts also compromises electrolytes' cost, ionic conductivity, density, wettability, and temperature compatibility. In this study, we propose a competitive solvation strategy to expand the electrochemical window of aqueous KCF_3SO_3 electrolyte up to 3.2 V with low salt concentration (i.e., 1–2 m), avoiding the use of excessive salts and tackling the challenges of super-concentrated electrolytes. Our findings indicate that various aprotic solvents

* Corresponding author.
** Corresponding author.
E-mail addresses: shuilinwu2-c@my.cityu.edu.hk (S. Wu), apwjzh@cityu.edu.hk (W. Zhang).
[1] Yibing Yang and Jiapei Li are equally contributed.

https://doi.org/10.1016/j.jpowsour.2025.236925
Received 13 January 2025; Received in revised form 4 March 2025; Accepted 28 March 2025
Available online 23 April 2025

have different capability in modulating the water content in the primary solvation sheath and expanding the electrolytes' electrochemical stable window, which is determined by the aprotic solvents' negative charge distribution and binding energy with K^+ cations. The supercapacitor prototype using a 2 m KCF_3SO_3-trimethyl phosphate/H_2O electrolyte achieves an operating voltage of 2.6 V, with a 70 % improvement in energy density than that of aqueous KCF_3SO_3 electrolyte (2.0 V). Additionally, the supercapacitor demonstrated excellent cyclic stability, with 81 % capacitance retention after 100, 000 cycles, along with wide temperature compatibility.

1. Introduction

Aqueous electrolytes have emerged as a promising alternative to traditional organic electrolytes in energy storage systems due to their numerous advantages, particularly in terms of safety, cost-effectiveness, and environmental impact [1–4]. These advantages position aqueous electrolytes as a key technology for developing safer, more sustainable, and cost-effective energy storage systems that meet the growing demands with stringent safety requirements. However, the narrow electrochemical stable window of water (~1.23 V) limits the energy density of aqueous-based energy storage system. For instance, in electrochemical double-layer supercapacitors (EDLCs), the energy density is proportional to the square of its operating voltage ($E=1/2\ CV^2$) [5]. Improving the operation voltage by a factor of two can result in a four-fold increase in energy density. Therefore, expanding the electrochemical window of water is critical for the practical application of aqueous-based energy storage systems.

Recently, various strategies have been developed to broaden the electrochemical stable windows of aqueous electrolytes, such as building 'water in salt' electrolytes [6], [-18] forming deep eutectic electrolytes [19–25], and introducing molecular crowding agents [26–28]. For example, high concentrations of highly soluble salts (*e.g.*, fluorine-containing salts [7–10], perchlorate salts [16,29], acetate salts [12]) have been dissolved in water to create 'water in salt' electrolytes. In these electrolytes, most water molecules are solvated with excessive cations/anions, effectively suppressing water decomposition due to enhanced interactions between water molecules and electrolyte ions. Similarly, non-solvents (*e.g.*, sugar, urea, and methanol) with high solubility have also been introduced into aqueous electrolytes to form deep eutectic electrolytes, thereby expanding the electrochemical window of water through strengthening the interactions with water molecules [21, 30,31]. While 'water in salt' and deep eutectic electrolytes can effectively broaden the electrochemical stable window, these super-concentrated electrolytes often face challenges such as low ionic

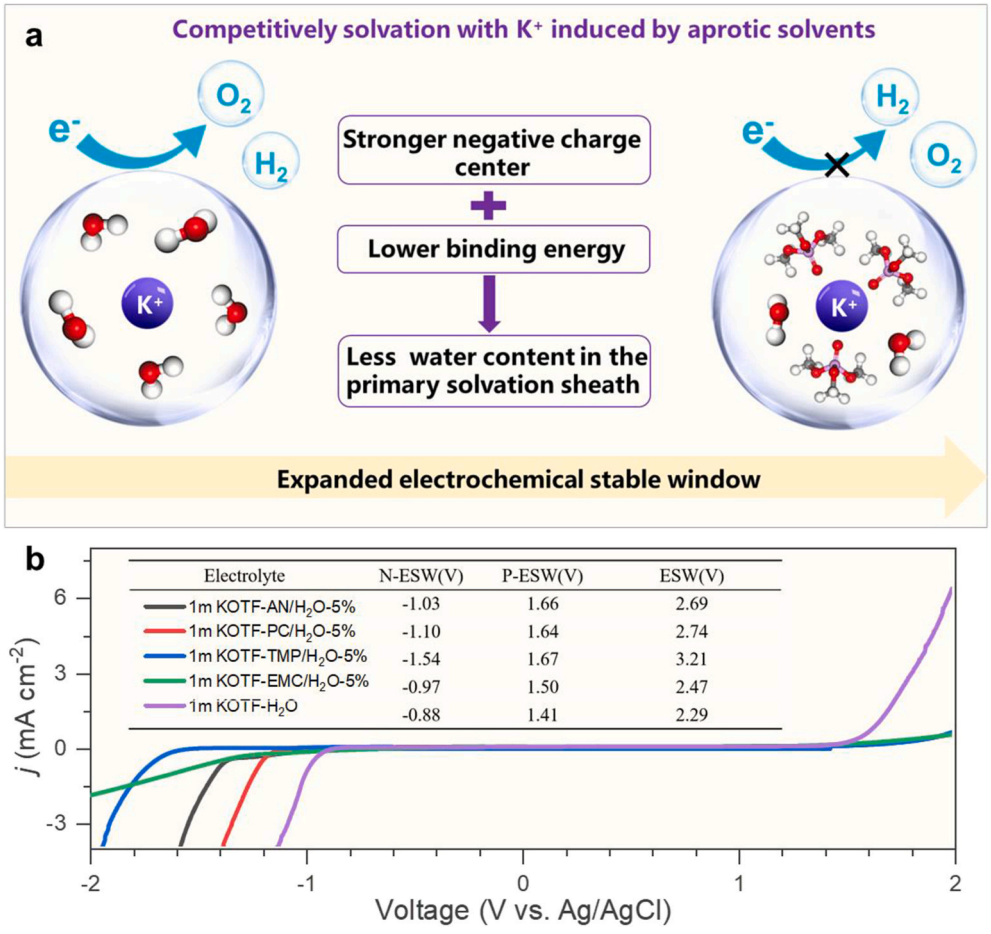

Fig. 1. (a) Schematic illustration of the competitive solvation of aprotic solvents with K^+ cations. Aprotic solvents, with strong negative charge centers and low binding energy with K^+ cations, competitively solvate K^+ cations while excluding water molecules from the primary solvation sheath. This exclusion suppresses charge transfer on water molecules, thereby expanding the electrochemical window of water. And (b) the LSV curves characterizing the electrochemical stable window of different electrolytes. The electrochemical stable window is summarized in the insert table, in which the negative and positive electrochemical stable window (N-ESW and P-ESW) of the electrolyte is defined with the current density below 100 μA cm^{-2} in the LSV curves.

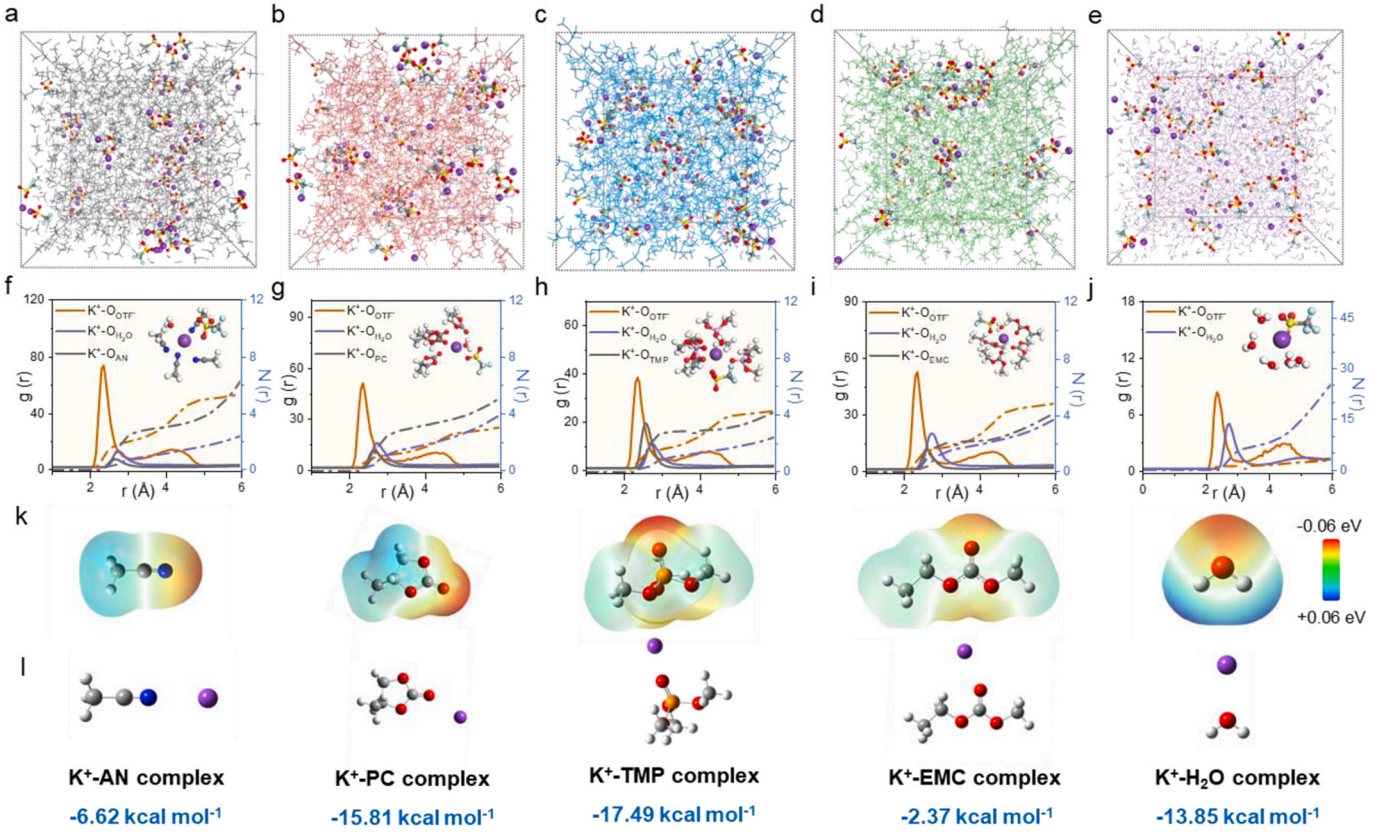

Fig. 2. Snapshots of the solvation structures from molecule dynamics simulation of (a) 1m KOTF-AN/H_2O-5 %, (b) 1m-KOTF-PC/H_2O-5 %, (c) 1m-KOTF-TMP/H_2O-5 %, (d) 1m-KOTF-EMC/H_2O-5 %, and (e) 1m-KOTF-H_2O electrolytes. The RDFs and coordination numbers for (f) 1m KOTF-AN/H_2O-5 %, (g) 1m KOTF-PC/H_2O-5 %, (h) 1m KOTF-TMP/H_2O-5 %, (i) 1m KOTF-EMC/H_2O-5 %, and (j) 1m KOTF- H_2O electrolytes. Insets are their representative solvation structures of the K^+ primary solvation shell. (k) The ESP maps of different aprotic solvents. (l) Coordination structures and binding energies of K^+-solvent complexes. Color scheme of atoms: K-purple, C-gray, H-white, N-blue, O-red, and P-orange. (For interpretation of the references to colour in this figure legend, the reader is referred to the Web version of this article.)

conductivity, high viscosity, and poor wettability, which can compromise the rate capability of EDLCs [3,32]. Additionally, the use of excessive salts inevitably increases the electrolyte density, adding weight to devices and potentially decreasing overall energy density [3]. Therefore, new approaches to expand the electrochemical window of aqueous-based electrolytes at low salt concentrations are essential to address these challenges. Furthermore, the developed aqueous electrolytes should also possess wide temperature compatibility, particularly given the high freezing point and volatility of water.

In general, cations in electrolytes are considered as Lewis acids, while water acts as a strong Lewis base due to its high electron-donating ability [33,34]. As a result, water molecules tend to solvate cations, forming a water-rich primary solvation sheath in dilute aqueous electrolytes. When this sheath migrates to the electrode interface, electrons can easily transfer to the water, triggering hydrogen or oxygen evolution reactions and leading to a narrow electrochemical stable window. The aprotic solvents with high donor numbers, like water, can also be considered as Lewis bases, but they offer a much wider electrochemical window. These solvents are anticipated to competitively solvate cations and displace water from the primary solvation sheath, thereby expanding the electrochemical window [35–38]. Previous studies, including those by Yan's group and our own, have introduced acetonitrile and trimethyl phosphite (TMP) into aqueous electrolytes, achieving operational voltages of up to 2.2 V and 2.4 V in EDLC prototypes, respectively [39–41]. Albeit aprotic solvents have been verified to be able to expand aqueous-based electrolytes' electrochemical window, the capabilities and affecting factors of aprotic solvents in modulating the electrochemical stable window lack systematic investigations. Moreover, the operation voltages of the EDLCs are needed to be further improved to achieve satisfactory energy density.

In this work, we introduced several aprotic solvents (*e.g,* acetonitrile, propylene carbonate, ethyl methyl carbonate, and trimethyl phosphite) with distinct characteristics into aqueous KOTF electrolytes and comprehensively studied their effectiveness in tuning the electrochemical stable windows of the electrolytes. The results show that these aprotic solvents can competitively solvate K^+ cations and partially exclude water molecules from the electrolyte's primary solvation sheath, thereby expanding the electrochemical stable window (Fig. 1a). The charge distributions of the aprotic solvents and their binding energies with K^+ cations are identified to be key factors in modulating the electrolyte's electrochemical stable window. Among these aprotic solvents, the TMP, with its strong negative charge center and low binding energy with K^+ cations, demonstrated the greatest effectiveness in expanding the electrochemical window of water, and the optimized electrolyte composition (2 m KOTF-H_2O/TMP-5 %) achieved a wide electrochemical window of up to 3.2 V. A prototype of EDLCs utilizing this electrolyte exhibited excellent performance, including a high operation voltage of 2.6 V, long cyclic stability with 81 % capacitance retention after 100, 000 cycles, and broad temperature compatibility (−10 °C to 60 °C). These results provide insights for designing new aqueous-based electrolytes for high-performance EDLCs.

2. Results and discussion

The electrochemical stable windows of the 1m KOTF aqueous electrolyte incorporating various aprotic solvents (*i.e.*, AN, PC, EMC, and

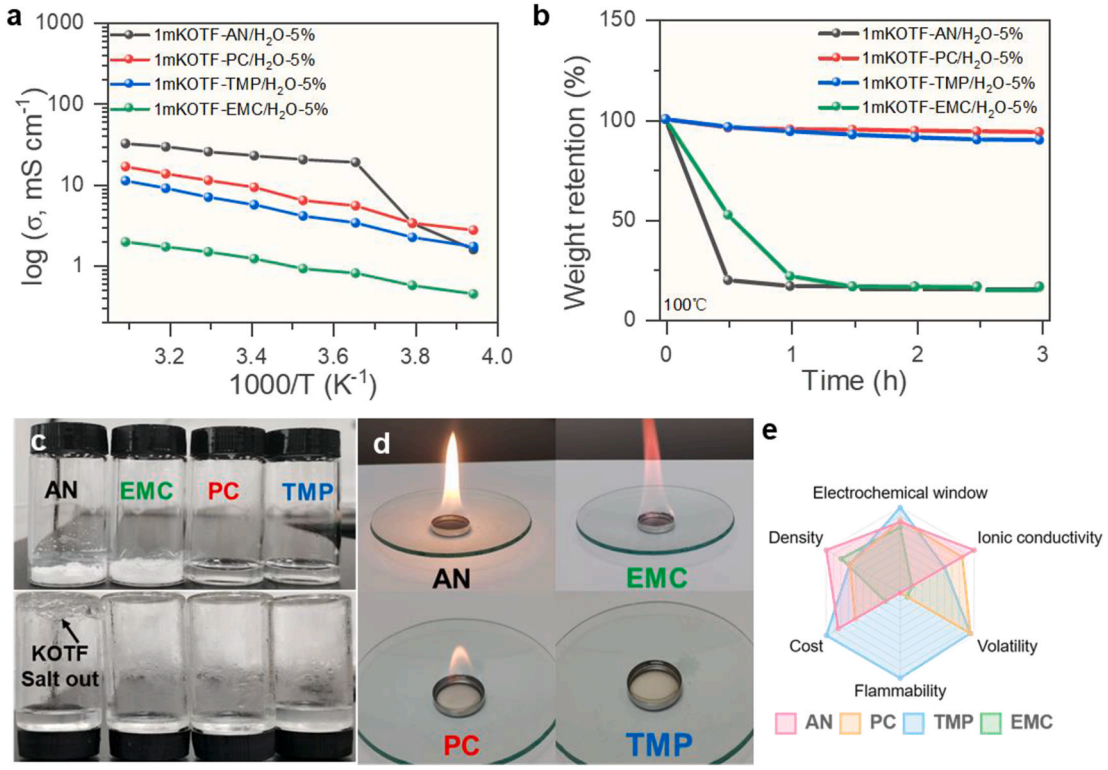

Fig. 3. Physical characteristics of the 1m KOTF electrolytes incorporated with different aprotic solvents. (a) Ionic conductivities of the electrolytes at different temperatures (−20 °C–50 °C), (b) weight retention of different electrolytes at 100 °C, (c) digital photographs of the electrolytes after treatment at 100 °C and −20 °C for 2 h, (d) flammability tests of the different electrolytes, and (e) radar charts of the characteristics of the electrolytes.

TMP) were initially evaluated using linear sweep voltammetry (LSV) technique. The LSV curves (Fig. 1b) indicate that the hydrogen evolution and oxygen evolution reactions of water confine the lower and upper potential limits of the electrolyte, respectively; thus defining the electrolytes' electrochemical stable window, as summarized in the inset table of Fig. 1b. Notably, the incorporation of aprotic solvents effectively expands the electrochemical stable windows to 2.5–3.2 V, in sharp contrast to the 1m KOTF aqueous electrolyte, which has an electrolyte stable window of 2.3 V. Moreover, different aprotic solvents show distinct capabilities in regulating the electrochemical stable window, with the sequence of TMP > PC > AN > EMC.

In order to clarify the capability difference of these aprotic solvents in modulating the electrolytes' electrochemical stable window, molecular dynamic simulations were employed to investigate the evolution of the primary solvation sheath of the electrolytes after introducing different aprotic solvents. The snapshots of the solvation structures around K^+ cations in these electrolytes (Fig. 2a–e) are much different, indicating the introduction of aprotic solvents can remarkably regulate the solvation structures. Moreover, the radial distribution functions (RDF) and coordination numbers of these electrolytes (Fig. 2f–j) are analyzed to quantitatively compare the coordinations of solvents and anions with the K^+ cations. The results indicate that the introduction of aprotic solvents can remarkably reduce the coordination numbers of water from 4.69 in 1m KOTF-H_2O to 0.64–1.38 in the first solvation shell of K^+, verifying the competitive solvation effect of aprotic solvents. The coordination numbers in the K^+ primary solvation sheath (r < 3 Å) are also summarized in Fig. S1 (Supporting Information). The coordination number in MD simulations depends on both solvent binding strength and number density, which is influenced by molecular weight. Due to TMP's higher molecular weight than AN, fewer TMP molecules are available at the same mass fraction, leading to a slightly higher apparent K^+-H2O coordination number than that of AN based electrolyte. In addition, while K^+-OTF^- coordination may be affected by solvent choice, this study primarily focuses on solvent-regulated K^+ solvation and electrochemical window expansion, which are more critical for EDLC performance. The drastically reduced coordination numbers between water and K^+ cations and increased coordination numbers between aprotic solvent and K^+ cations again verify the competitive solvation effect of aprotic solvents. Additionally, the Raman spectroscopy (Fig. S2, Supporting Information) and the Fourier Transform Infrared (FT-IR) spectroscopy (Fig. S3, Supporting Information) further corroborate the above findings. In particular, the peak intensity corresponding to the –OH group in water molecules drastically decreased after the introduction of aprotic solvents, indicating the disruption of pristine hydrogen bonds among water molecules induced by the aprotic solvents.

The charge distribution of the aprotic solvents, especially the presence of negative charge centers, is crucial for their binding strength and sites and with K^+ cations, which greatly affects their coordination capabilities with K^+ cations. Thus, the electrostatic potential (ESP) maps and the minimum ESP valve (ESP_{min}) of different aprotic solvents and their binding energies with K^+ cations are further calculated through the density functional theory. For the aprotic solvents, negative charges are primarily located on the C=O, C ≡ N, and P=O groups from the PC, EMC, AN and TMP, respectively, with the dark red region indicating a strong tendency to solvate with K^+ cations (Fig. 2k). The lower ESP_{min} values of TMP and PC indicate their stronger negative charge centers, making them more competitive in solvating K^+ compared to water. The coordination structures of the K^+-solvent complex further verified the solvation sites, and the binding energies depicted the solvation strength of different solvents with K^+ cations, as shown in Fig. 2l. Specifically, TMP demonstrated the lowest binding energy (−17.49 kcal mol^{-1}) with K^+ cations, which is notably lower than that of water molecules (−13.85 kcal mol^{-1}), indicating TMP's superior solvation capability. By contrast, EMC exhibited much higher binding energy (−2.37 kcal mol^{-1}) with K^+ cations, revealing its poor solvation capability with K^+ cations. These results suggest that the strong negative charge center of solvents enables

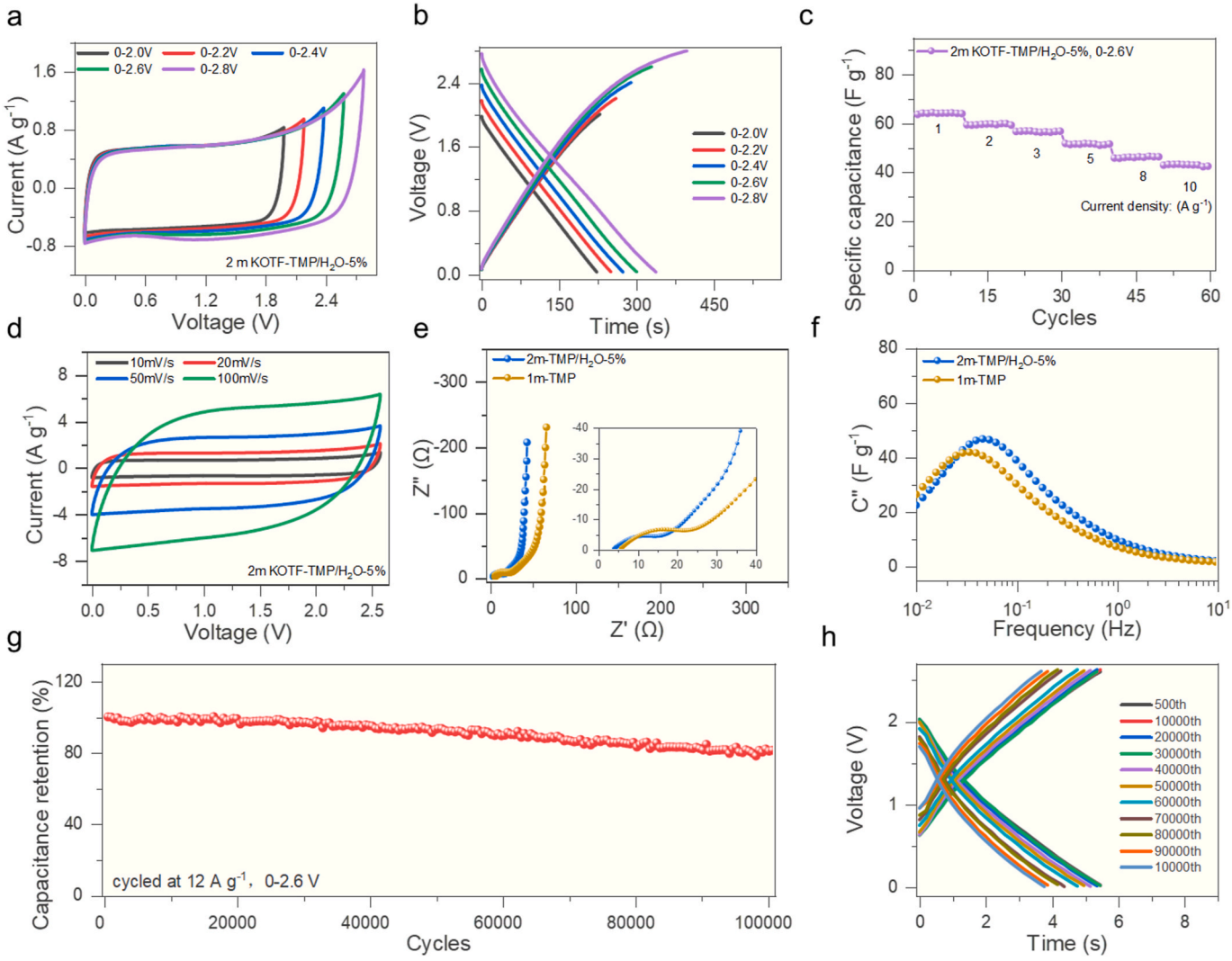

Fig. 4. Electrochemical performance of the AC-based EDLCs with the 2m KOTF-TMP/H_2O-5 % electrolyte at 25 °C. (a) Cyclic voltammetry curves of the EDLCs across different voltage ranges at 10 mV s^{-1}. (b) Galvanostatic charge-discharge curves of the EDLCs within different voltage ranges at 0.5 A g^{-1}. (c) Rate capability of the EDLCs with current densities increasing from 1 to 10 A g^{-1}. (d) Cyclic voltammetry curves with scan rates increasing from 10 mV s^{-1} to 100 mV s^{-1}. (e) Nyquist plots and (f) plots of imaginary specific capacitance versus frequency. (g) Cycle stability of the EDLCs in the 2m KOTF-TMP/H_2O-5 % electrolyte within 0–2.6 V at 12 A g^{-1}, and (h) the corresponding charge-discharge curves at specific cycles.

strong solvation capability with K^+ cations, thereby reducing the water content in the K^+ cation's primary solvation sheath through competitively solvation and electrochemical windows.

In addition to the narrow electrochemical window of aqueous electrolytes, their high sensitivity to temperature variation, due to the volatility and high freezing point of water, poses another challenge for practical applications. This issue can be effectively addressed by incorporating aprotic solvents. Notably, the electrolytes containing aprotic solvents (excluding acetonitrile) maintained decent ionic conductivities (2–31 mS cm^{-1}) over a broad temperature range (−20 °C–50 °C), in sharp contrast to the greatly decreased ionic conductivity of the 1m KOTF-H_2O and 1m-KOTF-AN/H_2O-5 % electrolytes below −10 °C (Fig. 3a). Moreover, the electrolytes' tolerance to high temperatures was evaluated based on their weight retention at the boiling point of water (Fig. 3b). The results demonstrated the superior water retention capabilities of PC and TMP. Digital photographs (Fig. 3c) of the electrolytes treated under 100 °C and −20 °C further verified the excellent temperature tolerance of the electrolytes containing PC and TMP. The flammability of these electrolytes was also tested (Fig. 3d), revealing that only the 1m-KOTF-TMP/H_2O-5 % electrolyte was fire-retardant. At the same time, in 1m-KOTF-TMP/H2O-5 %, the capacitance of the supercapacitor is significantly higher than that in other electrolytes. Thanks to the addition of TMP, the working voltage of the supercapacitor is significantly increased, while the rate performance is not significantly affected, achieving a good balance (Fig. S4, Supporting Information). Finally, the cost of each electrolyte was calculated (Fig. S5, Supporting Information), and the 1m-KOTF-TMP/H_2O-5 % electrolyte (1.2 $ ml^{-1}) was shown to be considerably less expensive than super-concentrated electrolytes (~15 $ ml^{-1}) and other electrolytes, while being slightly more expensive than the 1m KOTF aqueous electrolyte (0.9 $ ml^{-1}). In summary, incorporating TMP into aqueous electrolytes can effectively enhance the electrochemical window, cost efficiency, anti-flammability, and temperature compatibility of the aqueous KOTF electrolytes, as illustrated in the Radar chart in Fig. 3e.

To further assess the practical application of electrolytes, a prototype of electrochemical double-layer supercapacitors (EDLCs) was fabricated with commercial active carbon, and its electrochemical performance, specially operating voltage, cycle stability, and temperature compatibility, was systematically evaluated. Initially, the stable operating voltages of the EDLC prototype with various electrolytes were determined using galvanostatic charge-discharge (GCD) and cyclic voltammetry (CV) techniques (Fig. S6, Supporting Information). The results

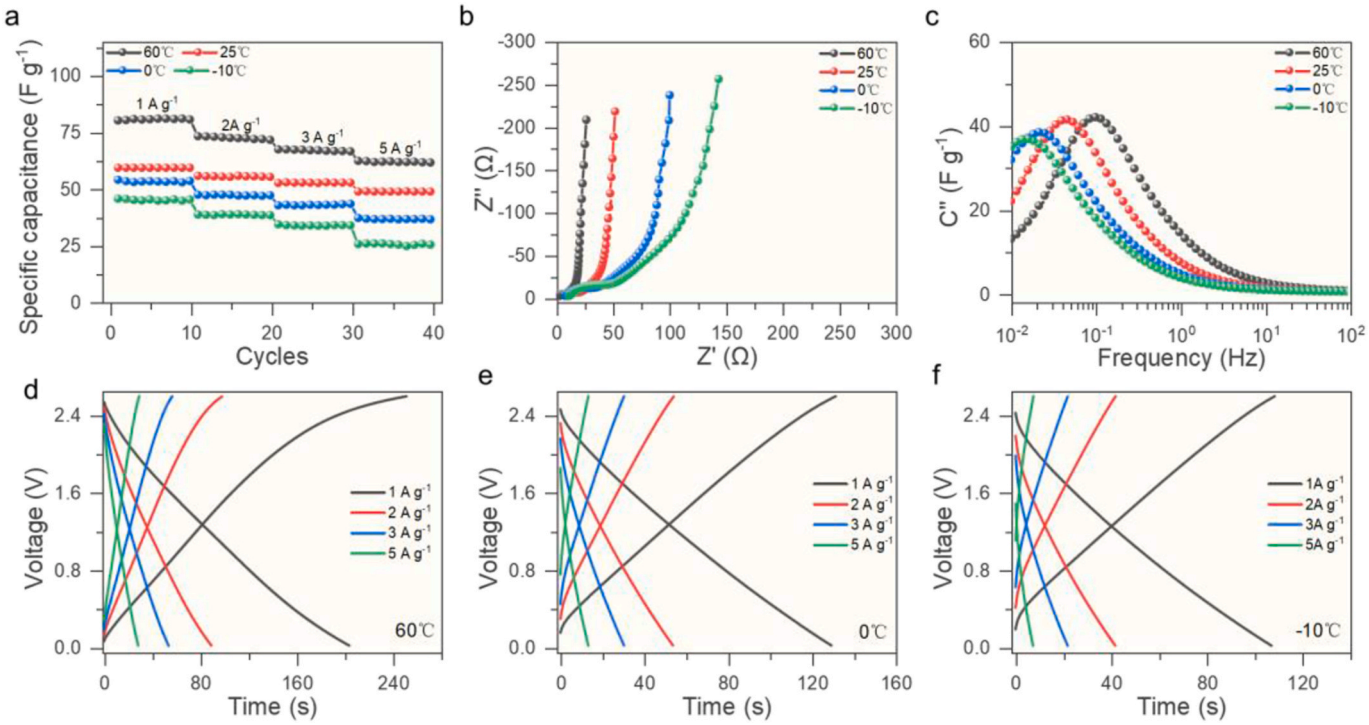

Fig. 5. Electrochemical performance of AC-based EDLCs with the 2m KOTF-TMP/H_2O-5 % electrolyte at different temperatures ranging from −10 to 60 °C. (a) Specific capacitance calculated from galvanostatic charge-discharge curves at various temperatures and current densities. (b) Nyquist curves at different temperatures. (c) The plots of impedance *vs*. frequency for the Warburg process at various temperatures. Galvanostatic charge-discharge curves at different current densities at (d) 60 °C, (e) 0 °C, and (f) −10 °C.

showed that the TMP-incorporated electrolytes exhibited the highest operation voltages up to 2.6 V in the EDLC prototypes. In a sharp contrast, the 1m KOTF aqueous electrolyte and 21m LiTFSI super-concentrated electrolyte can only enable an operation voltage up to 2.0 V and 2.2 V, respectively, as revealed by CV (Figs. S7a and S8a, Supporting Information) and GCD curves (Figs. S7b and S8b, Supporting Information). Additionally, the salt concentrations and water contents in the TMP-incorporated electrolytes were optimized to further enhance the electrochemical window and operation voltage. The LSV curves (Fig. S9, Supporting Information) revealed that the electrochemical stable window expanded with higher salt concentrations and lower water contents, with the 2 m KOTF-TMP/H_2O-5 % electrolyte showing the widest electrochemical window. The GCD and CV curves (Fig. 4a and b, and **S10**, Supporting Information) further verified the highest operating voltage of 2.6 V for the EDLC prototype using the 2 m KOTF-TMP/H_2O-5 % electrolyte.

Moreover, the EDLC prototype exhibited excellent rate capability with a capacitance retention of 66 % when the current density was increased from 1 A g^{-1} to 10 A g^{-1} (Fig. 4c). The CV curves (Fig. 4d) sustained a quasi-rectangular shape with minimal distortion as the scan rate increased from 10 mV s^{-1} to 100 mV s^{-1}, providing further evidence of the outstanding rate capability of the EDLC using the 2m-KOTF-TMP/H_2O-5 % electrolyte. The electrochemical impedance spectra (EIS) again confirmed the superior rate capability, as indicated by the low charge transfer resistance in the Nyquist curves (Fig. 4e) and the short relaxation time (τ_0) shown in the imaginary capacitance vs. frequency plot (Fig. 4f). In addition, the ionic conductivity of the 5 % water electrolyte is significantly higher than that of the anhydrous electrolyte within the temperature range of −20 °C–50 °C. Moreover, the rate capacity retention of the water-containing electrolyte is as high as 70 % (from 1 A g^{-1} to 10 A g^{-1}), while that of the anhydrous electrolyte is only 49 %. This demonstrates the superiority of adding 5 % water compared to not adding water to the electrolyte (Fig. S11, Supporting Information). Furthermore, the cyclic stability of the EDLCs with the 2m-KOTF-TMP/H_2O-5 % electrolyte was evaluated using the GCD technique over a voltage range of 0–2.6 V at 12 A g^{-1}. The results demonstrated excellent capacitance retention of 81 % after 100, 000 cycles (Fig. 4g and h). The slight increase in charged transfer resistance observed in the Nyquist plots (Fig. S12, Supporting Information) after 100, 000 cycles further validated the outstanding cyclic stability of the AC-based EDLC prototype with the 2m-KOTF-TMP/H_2O-5 % electrolyte, confirming the feasibility of this electrolyte for practical applications in EDLC devices.

The temperature-dependent electrochemical performance of the 2m-KOTF-TMP/H_2O-5 % electrolyte was also assessed based on the EDLCs over a temperature range of −10 °C to 60 °C. The results verified the broad temperature compatibility of the EDLCs with this electrolyte. Particularly, 70 % of the specific capacitance was maintained when the temperature decreased from 60 to −10 °C (Fig. 5a). Meanwhile, the rate capabilities of the EDLCs remained consistent across different operating temperatures. Moreover, the EIS results indicated only slight changes in charge transfer resistances and τ_0 at different temperatures (Fig. 5b and c), further verifying the wide temperature compatibility of the 2m-KOTF-TMP/H_2O-5 % electrolyte for EDLC applications. The galvanostatic charge-discharge curves of the EDLCs with the 2m-KOTF-TMP/H_2O-5 % electrolyte retained a linear and symmetric shape across the wide temperature range from 60 °C to −10 °C (Fig. 5d–f), demonstrating excellent capacitive behavior under diverse temperature conditions.

3. Conclusion

In summary, a range of aprotic solvents has been comprehensively studied to elucidate their varying capabilities in modulating the electrochemical windows of aqueous electrolytes. The distribution of negative charge in aprotic solvents and binding energy between these solvents and K^+ cations have been identified as key factors in regulating solvation structures and, consequently, the electrochemical windows of the electrolytes. Among the tested aprotic solvents, TMP exhibits the strongest negative charge center and the lowest binding energy with K^+

cations. This enables TMP to effectively coordinate with K^+ cations, thereby excluding water molecules from the primary solvation structures, as confirmed by molecular dynamic simulations. The significant reduction of water molecules in the primary solvation shells in the TMP incorporated electrolyte remarkably suppresses water decomposition, resulting in a substantially expanded electrochemical window. Moreover, the EDLC prototype utilizing the 2 m KOTF-TMP/H_2O-5 % can operate at a high voltage of up to 2.6 V and across a broad temperature range (−10 °C–60 °C), and demonstrates excellent cycle stability beyond 100, 000 cycles, as compared with other reports in Table S1 (Supporting Information). This work provides guidelines for screening aprotic solvents to expand the electrochemical window of aqueous electrolytes and for designing new electrolytes with tunable characteristics.

CRediT authorship contribution statement

Yibing Yang: Conceptualization. **Jiapei Li:** Data curation, Conceptualization. **Junlin Shi:** Conceptualization. **Fei Pan:** Data curation, Conceptualization. **Shuilin Wu:** Writing – review & editing, Writing – original draft, Conceptualization. **Daohong Zhang:** Conceptualization. **Yanwu Zhu:** Conceptualization. **Wenjun Zhang:** Conceptualization.

Declaration of competing interest

The authors declare that they have no known competing financial interests or personal relationships that could have appeared to influence the work reported in this paper.

Acknowledgments

This work was supported by the National Nature Science Foundation of China (22209211, 52172241, and 52372229), Hong Kong Research Grants Council (CityU 11310123, and CityU 11315622), the research funds from South-Central Minzu University (YZZ22001).

Appendix A. Supplementary data

Supplementary data to this article can be found online at https://doi.org/10.1016/j.jpowsour.2025.236925.

Data availability

Data will be made available on request.

References

[1] T.Z. Guo, D. Zhou, L.X. Pang, S.K. Sun, T. Zhou, J.Z. Su, Small 18 (16) (2022) 2106360.
[2] D.L. Chao, W.H. Zhou, F.X. Xie, C. Ye, H. Li, M. Jaroniec, S.Z. Qiao, Sci. Adv. 6 (21) (2020) eaba4098.
[3] D.L. Chao, S.Z. Qiao, Joule 4 (9) (2020) 1846–1851.
[4] O. Borodin, J. Self, K.A. Persson, C.S. Wang, K. Xu, Joule 4 (1) (2020) 69–100.
[5] F. Béguin, V. Presser, A. Balducci, E. Frackowiak, Adv. Mater. 26 (14) (2014) 2219–2251.
[6] J. Park, J. Lee, W. Kim, ACS Energy Lett. 6 (2) (2021) 769–777.
[7] L.M. Suo, O. Borodin, T. Gao, M. Olguin, J. Ho, X.L. Fan, C. Luo, C.S. Wang, K. Xu, Science 350 (6263) (2015) 938–943.
[8] L.M. Suo, O. Borodin, Y.S. Wang, X.H. Rong, W. Sun, X.L. Fan, S.Y. Xu, M. A. Schroeder, A.V. Cresce, F. Wang, C.Y. Yang, Y.S. Hu, K. Xu, C.S. Wang, Adv. Energy Mater. 7 (21) (2017) 1701189.
[9] L.W. Jiang, Y.X. Lu, C.L. Zhao, L.L. Liu, J.N. Zhang, Q.Q. Zhang, X. Shen, J. M. Zhao, X.Q. Yu, H. Li, X.J. Huang, L.Q. Chen, Y.S. Hu, Nat. Energy 4 (6) (2019) 495–503.
[10] Y. Yamada, K. Usui, K. Sodeyama, S. Ko, Y. Tateyama, A. Yamada, Nat. Energy 1 (2016) 16129.
[11] M.H. Lee, S.J. Kim, D. Chang, J. Kim, S. Moon, K. Oh, K.Y. Park, W.M. Seong, H. Park, G. Kwon, B. Lee, K. Kang, Mater. Today 29 (2019) 26–36.
[12] M.R. Lukatskaya, J.I. Feldblyum, D.G. Mackanic, F. Lissel, D.L. Michels, Y. Cui, Z. A. Bao, Energy Environ. Sci. 11 (10) (2018) 2876–2883.
[13] L.W. Jiang, L.L. Liu, J.M. Yue, Q.Q. Zhang, A.X. Zhou, O. Borodin, L.M. Suo, H. Li, L.Q. Chen, K. Xu, Y.S. Hu, Adv. Mater. 32 (2) (2020) 1904427.
[14] D. Reber, R. Grissa, M. Becker, R.S. Kühnel, C. Battaglia, Adv. Energy Mater. 11 (5) (2021) 2002913.
[15] D.P. Leonard, Z.X. Wei, G. Chen, F. Du, X.L. Ji, ACS Energy Lett. 3 (2) (2018) 373.
[16] J. Park, J. Lee, W. Kim, ACS Energy Lett. 7 (4) (2022) 1266–1273.
[17] J.M. Yue, L.D. Lin, L.W. Jiang, Q.Q. Zhang, Y.X. Tong, L.M. Suo, Y.S. Hu, H. Li, X. J. Huang, L.Q. Chen, Adv. Energy Mater. 10 (36) (2020) 2000665.
[18] Y. Zhang, J. Xu, Z. Li, Y.R. Wang, S.J. Wang, X.L. Dong, Y.G. Wang, Sci. Bull. 67 (2) (2022) 161–170.
[19] J.J. Xu, X. Ji, J.X. Zhang, C.Y. Yang, P.F. Wang, S.F. Liu, K. Ludwig, F. Chen, P. Kofinas, C.S. Wang, Nat. Energy 7 (2) (2022) 186–193.
[20] Z.G. Hou, M.F. Dong, Y.L. Xiong, X.Q. Zhang, Y.C. Zhu, Y.T. Qian, Adv. Energy Mater. 10 (15) (2020) 1903665.
[21] H.B. Bi, X.S. Wang, H.L. Liu, Y.L. He, W.J. Wang, W.J. Deng, X.L. Ma, Y.S. Wang, W. Rao, Y.Q. Chai, H. Ma, R. Li, J.T. Chen, Y.P. Wang, M.Q. Xue, Adv. Mater. 32 (16) (2020) 2000074.
[22] L. Geng, J. Meng, X. Wang, C. Han, K. Han, Z. Xiao, M. Huang, P. Xu, L. Zhang, L. Zhou, L. Mai, Angew. Chem. Int. Ed. 62 (22) (2023) 2206717.
[23] J.N. Hao, L.B. Yuan, Y.L. Zhu, X.W. Bai, C. Ye, Y. Jiao, S.Z. Qiao, Angew. Chem. Int. Ed. 62 (39) (2023) 2310284.
[24] Y.P. Zhu, X.R. Guo, Y.J. Lei, W.X. Wang, A.H. Emwas, Y.Y. Yuan, Y. He, H. N. Alshareef, Energy Environ. Sci. 15 (3) (2022) 1282–1292.
[25] R.W. Chen, C.Y. Zhang, J.W. Li, Z.J. Du, F. Guo, W. Zhang, Y.H. Dai, W. Zong, X. Gao, J.X. Zhu, Y. Zhao, X.H. Wang, G.J. He, Energy Environ. Sci. 16 (6) (2023) 2540–2549.
[26] J. Xie, Z. Liang, Y.-C. Lu, Nat. Mater. 19 (9) (2020) 1006–1011.
[27] D.J. Dong, J. Xie, Z.J. Liang, Y.C. Lu, ACS Energy Lett. 7 (1) (2022) 123–130.
[28] Y. Guo, J.X. Gu, R. Zhang, S.C. Zhang, Z. Li, Y.W. Zhao, Z.D. Huang, J. Fan, Z. F. Chen, C.Y. Zhi, Adv. Energy Mater. 11 (36) (2021) 2101699.
[29] X.D. Bu, L.J. Su, Q.Y. Dou, S.L. Lei, X.B. Yan, J. Mater. Chem. A 7 (13) (2019) 7541–7547.
[30] J.W. Zhao, J. Zhang, W.H. Yang, B.B. Chen, Z.M. Zhao, H.Y. Qiu, S.M. Dong, X. H. Zhou, G.L. Cui, L.Q. Chen, Nano Energy 57 (2019) 625–634.
[31] L. Ma, J. Vatamanu, N.T. Hahn, T.P. Pollard, O. Borodin, V. Petkov, M. A. Schroeder, Y. Ren, M.S. Ding, C. Luo, J.L. Allen, C.S. Wang, K. Xu, Proc. Natl. Acad. Sci. USA 119 (24) (2022) e2121138119.
[32] J.P. Xie, D.W. Lin, H. Lei, S.L. Wu, J.L. Li, W.J. Mai, P.F. Wang, G. Hong, W. J. Zhang, Adv. Mater. (2023) 2306508.
[33] J.E. Chen, H. Zhang, M.M. Fang, C.M. Ke, S. Liu, J.H. Wang, ACS Energy Lett. (2023) 2202478.
[34] P. Zhou, Y. Xiang, K. Liu, Energy Environ. Sci. (2024) D4EE02989E.
[35] D. Wang, T. He, A. Wang, K. Guo, M. Avdeev, C. Ouyang, L. Chen, S. Shi, Adv. Funct. Mater. 33 (11) (2023) 2212342.
[36] A.P. Wang, Z.Y. Zou, D. Wang, Y. Liu, Y.J. Li, J.M. Wu, M. Avdeev, S.Q. Shi, Energy Storage Mater. 35 (2021) 595–601.
[37] C. Zhang, Z. Cai, R. Huang, H. Pan, Batter. Supercaps 6 (2023) e202300053.
[38] Y.Y. Wang, Z.J. Wang, W.K. Pang, W. Lie, J.A. Yuwono, G.M. Liang, S.L. Liu, A. M. Angelo, J.J. Deng, Y.M. Fan, K. Davey, B.H. Li, Z.P. Guo, Nat. Commun. 14 (2023) 2720.
[39] Q.Y. Dou, S.L. Lei, D.W. Wang, Q.N. Zhang, D.W. Xiao, H.W. Guo, A.P. Wang, H. Yang, Y.L. Li, S.Q. Shi, X.B. Yan, Energy Environ. Sci. 11 (11) (2018) 3212–3219.
[40] D.W. Xiao, Q.Y. Dou, L. Zhang, Y.L. Ma, S.Q. Shi, S.L. Lei, H.Y. Yu, X.B. Yan, Adv. Funct. Mater. 29 (42) (2019) 1904136.
[41] S.L. Wu, B.Z. Su, M.Z. Sun, S. Gu, Z.G. Lu, K.L. Zhang, D.Y.W. Yu, B.L. Huang, P. F. Wang, C.S. Lee, W.J. Zhang, Adv. Mater. 33 (41) (2021) 2102390.